Application of Seismic Isolation Bearings in Aqueducts

Lin Xu, Junyi Huo*, Dahai Hu

School of Civil Engineering and Communications, North China University of Water Resources and Electric Power, Zhengzhou 450045, China

Corresponding Author Email: 18438609623@163.com

ABSTRACT

There are few examples of reducing and isolating technology used in oversize aqueduct at home and abroad. It is of great practical significance to study the seismic problem of large aqueduct and adopt safe, economical and reliable shock isolation and damping device to effectively reduce the impact of earthquake disaster. Based on the design and application of the shock absorber used in a beam aqueduct, and the mathematical model of the fluid-solid coupled finite element model, the seismic response of the extra-large earthquake isolation aqueduct is analyzed. The research results show that when using isolation bearings, the fundamental frequency is reduced by 82% compared to ordinary bearings, and the basic seismic period of the aqueduct structure is extended. Under the designed water depth condition, the main stress at the characteristic point decreased by 44.2%, and the deformation of the support increased by 32 mm. The curve was relatively full, indicating that the support has good dissipation capacity. The shear force and bending moment values at the bottom section of the pier pier have also significantly decreased, with a maximum reduction of 51.1% and 63.1%, respectively. The isolation bearings have played a good role in reducing and isolating earthquakes, improving the overall seismic safety of the aqueduct structure.

1. INTRODUCTION

The scale of aqueducts in the South to North Water Diversion Project is generally relatively large (For example, the Caohe aqueduct in the middle route of the South to North Water Diversion Project has a total length of 2300 m, a bottom width of 21.3 m, and a maximum span of 30 m; and the Shahe beam type aqueduct has a length of 1666 m, a single channel diameter of 8 m, and a net height of 7.4 m.), and the safe operation of these super large aqueducts plays a crucial role in ensuring the safe water transportation of the entire South to North Water Diversion Project. The safe use of large and special aqueducts is crucial [1]. Improving the seismic performance of large aqueduct structures by introducing seismic isolation devices has become a hot research and application topic in recent years.

Aqueduct is a kind of overhead water conveying structure, which has many similarities with bridge, so the research results of bridge vibration reduction and isolation can be used for reference in the research of aqueduct [2]. Bridge vibration isolation device can be divided into seismic bearing, vibration isolation bearing, damper and vibration isolation expansion device. In addition, in the design of bridge, the vertical force and horizontal force are separated to form a separated bearing. Common bearings include "ordinary bearings+rubber isolation bearings", "ordinary bearings+dampers", "ordinary bearings+horizontal force bearings", etc.

The seismic reduction and isolation devices in aqueducts mainly use isolation bearings to play a role in seismic and seismic reduction of the structure. The seismic reduction measures adopted in bridge engineering in China are mainly applied to plate rubber bearings, polytetrafluoroethylene sliding plate bearings, lead rubber bearings, pot type rubber seismic fixed bearings, and damping seismic spherical bearings [3, 4]. In 2014, Wang et al. [5] obtained the hysteresis curve of the lead rubber bearing by using ADINA software, and proved that it was in good agreement with the test curve, which verified the correctness of the numerical simulation. Then the support is applied to the seismic analysis of aqueduct, which shows that the seismic isolation effect is obvious and the seismic performance of aqueduct structure is effectively improved. In 2016, Ding [6] adopted the nonlinear time-history analysis method to compare and analyze the isolation and damping effects of lead rubber bearing, high-damping rubber bearing and hyperboloid spherical bearing, and believed that hyperboloid spherical bearing had the best damping effect. In 2019, He et al. [7] took a certain aqueduct as the research object, considered the seismic isolation and damping devices in bridge seismic design, and combined with the characteristics of the aqueduct itself, introduced friction pendulum isolation bearings for design analysis of the aqueduct. They believed that the friction pendulum isolation bearings had a significant seismic energy dissipation effect, which could significantly reduce the bending moment at the bottom of the pier and the displacement at the top of the pier, improve the stress on the lower structure, and make the pier basically meet the performance goals under the design earthquake. Zhang et al. [8] introduced the high-damping rubber bearing into the aqueduct structure, improved the Wilson-θ method, and carried out the elastic-plastic analysis of the aqueduct system. Combined with the dynamic characteristics and structural response, the seismic

characteristics of the high-damping bearing were studied. Han et al. [9] conducted elastic-plastic dynamic time history analysis on a certain aqueduct of the Dianzhong Water Diversion Project using basin type rubber bearings, lead core rubber bearings, and friction pendulum bearings. The impact of water level changes on the aqueduct structure and the vibration isolation effect of different bearings were analyzed.

2. FLUID-STRUCTURE COUPLING MODEL FOR SEISMIC ISOLATION OF AQUEDUCTS

2.1 Fluid-structure coupling model

Large aqueducts are mostly variable cross-section thin-walled reinforced concrete structures or prestressed reinforced concrete structures with supporting piers. The structure of the aqueduct is not rigid, and it is necessary to consider the fluid solid coupling effect between the entire aqueduct structure, including the supporting piers, and the water body inside the aqueduct. The commonly used treatment methods for fluid structure coupling problems currently include additional mass model, Housner equivalent mass spring model, displacement pressure finite element format, design standard model, etc.

The added mass model does not consider the liquid surface sloshing and compressibility of the water body. Because this method is simple in calculation, it is widely used in the initial stage. Under the assumption that the water body is incompressible and unshakable, the influence of the dynamic interaction between the aqueduct structure and the water body inside the aqueduct can be considered as an additional mass. According to the method of structural dynamic water pressure and additional mass, when analyzing the natural vibration characteristics of the aqueduct structure, the mass of water per unit area on one side of the aqueduct body in semi-infinite water can be calculated using the following formula:

$$M_w(z) = 7\eta\rho\sqrt{hz} / (8g) \tag{1}$$

where, $M_w(z)$ is the additional mass at the water surface distance from z; z is the distance from the calculation surface to the water level; h is the water depth in the aqueduct; ρ is the density of water body; η is the reduction coefficient. When applied in finite waters, the formula should be multiplied by a reduction factor.

The total additional mass per unit width of the water body acting on one side of the trough within z depth is:

$$M(z) = 7\eta\rho\sqrt{hz} / (12g) \tag{2}$$

The additional mass method of hydrodynamic pressure derived from Laplace's equation is widely used. When the water body interacts with the structure, an additional mass matrix is added on the basis of the mass matrix to realize the impact of fluid mass on solids. The finite element dynamic analysis equation considering the additional mass is:

$$[K]\{\delta\} + [C]\{\dot{\delta}\} + ([M] + [M_p])\{\ddot{\delta}\} = \{R_0\} \tag{3}$$

where: $[M]$ is the mass matrix; $[M_p]$ is the additional mass matrix; $\{R_0\}$ is a structural node load array that does not

consider dynamic water pressure loads; $[K]$ is the overall stiffness matrix; $[C]$ is the damping matrix; δ, $\dot{\delta}$ and $\ddot{\delta}$ are displacement, velocity, and acceleration vectors, respectively.

It can be seen that although the forms of additional mass are different, they only reflect the influence of dynamic water pressure on the structure, and ignore the compressibility and sloshing of the water body. The additional mass is only an approximate treatment method with certain defects.

The "Seismic Design Standards for Hydraulic Structures" [10] (hereinafter referred to as the "Design Standards") proposes an engineering practical method based on the finite element method to solve the seismic response of water bodies in large aqueducts. Introducing springs to simulate pulse pressure and convective pressure, the effect of convective hydrodynamic pressure inside the tank can be considered as a spring mass system connected to the inner wall of the aqueduct at height. The calculation diagram is shown in Figure 1, the equivalent mass M_1, the equivalent stiffness K_1 and height h_1 of the spring, can be calculated according to the following equation:

$$M_1 = 2\rho Hl\left[\frac{1}{3}\sqrt{\frac{5}{2}}\frac{l}{H}\tanh\left(\sqrt{\frac{5}{2}}\frac{H}{l}\right)\right] \tag{4}$$

$$K_1 = M_1\frac{g}{l}\sqrt{\frac{5}{2}}\tanh\left(\sqrt{\frac{5}{2}}\frac{H}{l}\right) \tag{5}$$

$$h_1 = H\left[1 - \frac{\cosh\left(\sqrt{\frac{5}{2}}\frac{H}{l}\right) - 2}{\sqrt{\frac{5}{2}}\frac{H}{L}\sinh\left(\sqrt{\frac{5}{2}}\frac{H}{l}\right)}\right] \tag{6}$$

In the formula: ρ is the mass density of the water body; H is the depth of water in the groove; l is half the width of the aqueduct; G is the acceleration of gravity; L is the width of the aqueduct.

Under the action of vertical seismic components, only the impact hydrodynamic pressure can be considered. The effect of water on the bottom of the aqueduct can be considered as a vertically uniformly distributed additional mass fixed on it, calculated according to Eq. (7); The effect of water on the aqueduct wall can be considered as the horizontal pressure distributed along the elevation, calculated according to Eq. (8). It should be noted that the hydrodynamic pressure acting on the relative groove wall at all times points in the same direction.

$$m_{wv} = 0.4\frac{M}{l} \tag{7}$$

$$p_{wv}(z,t) = 0.4\frac{M}{l}\alpha_{wv}(t)\cos\left(\frac{\pi}{2}\frac{H+z}{H}\right) \tag{8}$$

Based on the appeal understanding, the design standard model recommended in literature [10] was finally adopted in this paper to simulate the fluid-structure interaction and conduct modal analysis of the structure.
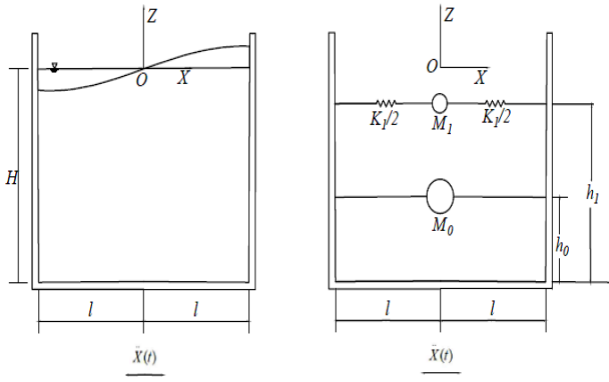
Figure 1. Schematic diagram of the dynamic water pressure calculation model

2.2 Model for restoring force of shock absorption support

This article selects HDR (I) - d970×369-G1.2 as the vibration isolation support, the performance parameters of the support are shown in Table 1. Simulate high damping supports using adjustable damping spring elements. Each bearing is simulated by three spring systems, the vertical spring adopts a linear model, and the horizontal two direction springs adopt a bilinear model. The bilinear restoring force model of this support is shown in Figure 2.

Table 1. Isolation support parameters

parameter	value	parameter	value
Design shear displacement of support (mm)	170	Initial horizontal stiffness (kN/mm)	16.21
Allowable shear displacement of support (mm)	425	Horizontal stiffness after yielding (kN/mm)	2.49
Ultimate shear displacement of support (mm)	595	Equivalent damping ratio (%)	0.15
Horizontal yield force of support (kN)	294	Vertical compressive stiffness (kN/mm)	1339
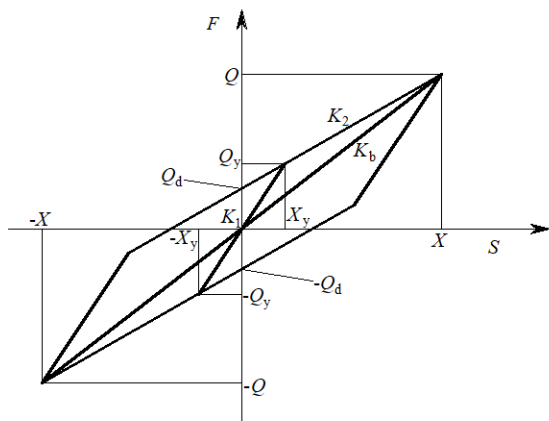
Figure 2. Frictional pendulum support bilinear hysteresis model

3. FINITE ELEMENT MODEL CALCULATION OF TYPICAL CASE

3.1 Finite element calculation model

A large aqueduct has a total length of 282.659m and a rectangular structure. It is made of C50 prestressed reinforced concrete, with a single span length of 25m and a total of 7 spans. The net size of the groove section is 4.9m×5.17m (width × Height), thickness of groove body: bottom plate 0.45m, side walls on both sides 0.4m, and upper flange 0.3m. The lower part of the aqueduct is supported by C30 reinforced concrete hollow piers and double column piers, and the supporting structures at both ends are C20 concrete piers and abutments. The aqueduct is equipped with 5 hollow piers and 1 double column pier. The height of the double pillar pier is 6.85m, which is composed of reinforced concrete square columns with length and width of 1.2m. The pier top is equipped with a cap of 1.9m×5.7m×0.8m (length × width × thickness). The trough pier foundation is made of C30 reinforced concrete, and the base size is 4.4m × 8.6m×1.6m (length × width × thickness). The hollow pier is 20m high, the wall thickness is 0.6m, the pier cap is 2.4m×5.7m×0.8m (thick × length × width), the trough pier foundation is made of C30 reinforced concrete, and the base size is 9.6×6.4m×1.6m (length × width × thickness). The three-dimensional finite element model is shown in Figure 3. Select feature points to analyze the dynamic time history results, and the distribution of feature points is shown in Figure 4.
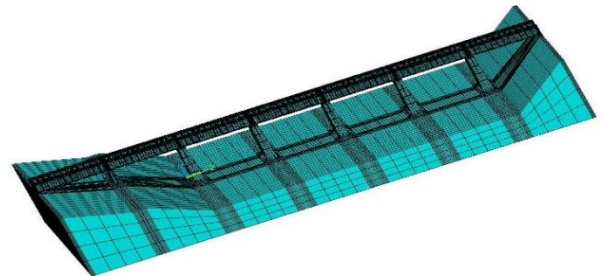
Figure 3. Global finite element model
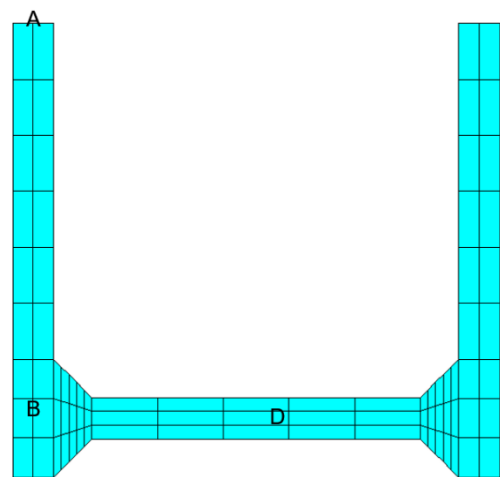
Figure 4. Feature point

3.2 Seismic wave selection

According to the geological survey report of the site, this aqueduct is located in the earthquake area with the basic

intensity of VIII degree. The peak acceleration of ground motion exceeding 10% probability within the base period (50 years) is adopted as the design peak acceleration of ground motion, the design peak horizontal acceleration is 0.3g, the damping ratio is 0.05, and the envelope line is taken as Jennings type envelope. The time history of synthetic artificial simulated earthquake acceleration is shown in Figure 4. By analyzing the comparison graph between the response spectrum of each set of artificial simulated seismic acceleration and the response spectrum curve of standard design, it can be found that the time history of man-made seismic acceleration meets the requirements of the seismic Standard. The required Seismic wave is synthesized according to the target response spectrum, as shown in Figure 5.
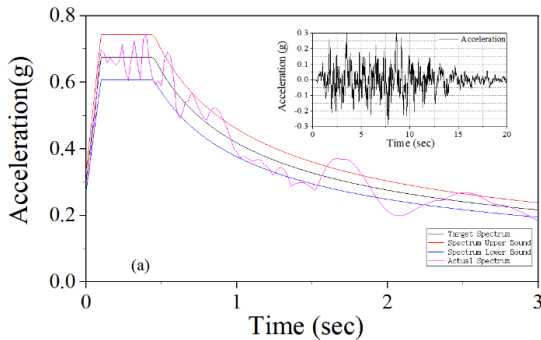
Figure 5. Seismic response spectrum

3.3 Analysis of dynamic characteristics

This article uses the Block Lanczos Method to solve the dynamic characteristics of large aqueducts and analyze their natural frequencies and main modes of vibration. Use finite element software to conduct modal analysis on the aqueduct and obtain the first six frequencies and vibration modes of the aqueduct. The natural frequencies and periods of the aqueduct are shown in Tables 2 and 3, respectively, and the vibration mode is shown in Figure 6.

Table 2. Frequency of each vibration order

Frequency order	Frequency /Hz		Frequency reduction /%
	Common support	Isolation support	
1	4.323	0.967	77.62
2	4.391	1.171	73.35
3	4.451	1.221	72.54
4	4.603	1.321	71.42
5	4.836	1.559	66.75
6	5.031	2.044	59.37

Table 3. Period of each vibration order

Frequency order	Period /s		Period extension /%
	Common support	Isolation support	
1	0.231	1.033	347.18
2	0.228	0.853	274.47
3	0.225	0.818	263.73
4	0.217	0.756	248.66
5	0.206	0.641	211.31
6	0.198	0.489	147.07

The first-order mode of the aqueduct is shown in Figure 6(a). It can be seen from the mode figure that the body of the

aqueduct exhibits translational motion along the direction of water flow. The second order mode is shown in Figure 6(b), and the body of the aqueduct shows a vertical motion trend. The third order mode of the aqueduct is shown in Figure 6(c). The body of the aqueduct shows a trend of vertical motion. Figure 6(d) shows the fourth order mode of the aqueduct. The body of the aqueduct vibrates in the X-Z plane. Figure 6(e) shows the fifth order mode of the aqueduct, and the body of the aqueduct shows an S-shaped vibration shape. Figure 6(f) shows the sixth order vibration mode of the aqueduct, and the body of the aqueduct shows an S-shaped vibration shape.

By analyzing the content shown in Table 3, it can be concluded that the stiffness of the structural system of a large aqueduct is reduced after the installation of isolation bearings, resulting in a significant reduction in the first six natural frequencies of the aqueduct structure, with a maximum reduction of about 73.5%. This prolongs the natural vibration period of the structure, successfully avoiding the scope of seismic energy concentration and reducing the seismic response of the aqueduct structure. This "reducing stiffness and increasing flexibility" technical method has shown good isolation effects.

(a) 1st vibration mode	(b) 2st vibration mode	(c) 3st vibration mode
(d) 4st vibration mode	(e) 5st vibration mode	(f) 6st vibration mode
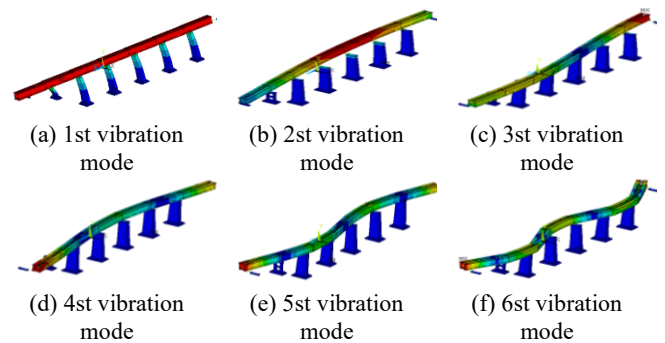
Figure 6. Vibration diagram

3.4 Analysis of dynamic calculation results

Input the seismic excitation into the water and no water conditions for dynamic response analysis, and provide the structural stress cloud map at the moment of the maximum first principal stress, as shown in Figure 7; Provide the hysteresis curve diagram of the support, as shown in Figure 8; Provide the displacement and stress time history curve of the characteristic points, as shown in Figure 9.

From the first stress cloud diagram 7 (a), it can be seen that the extreme value of the first principal stress of the aqueduct body under the empty channel condition is 20.3MPa, which occurs near the time of 15.78s. The location where the maximum stress occurs is at the support, which is caused by the stress concentration phenomenon at the support. From the first stress cloud diagram (b), it can be seen that the extreme value of the first principal stress in the aqueduct body under the design water depth condition is 2.07MPa, which occurs near the time of 13.92s. The location where the maximum stress occurs is also at the support, which is also caused by the stress concentration phenomenon at the support.

According to the concrete design specifications, the standard tensile strength of C50 concrete is 2.64MPa. As can be seen from Figure 7, the first principal stress in most areas of the groove body under two working conditions is between 0MPa~2.01MPa, that is, between the standard compressive strength and tensile strength of C50 concrete.

(a) Empty slot

(b) Design water depth
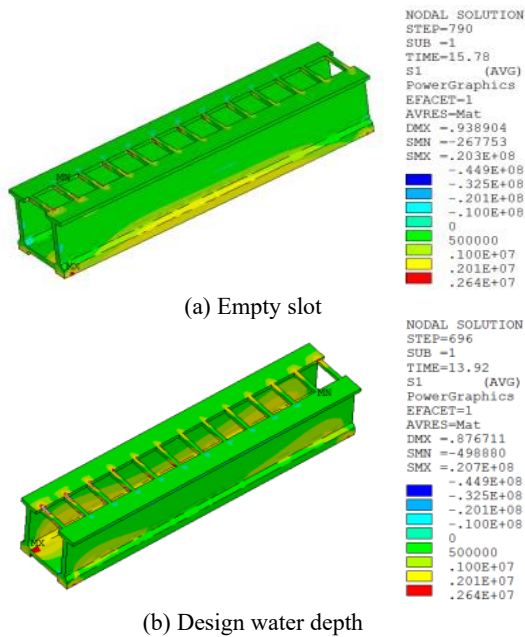
Figure 7. First principal stress cloud diagram

(a) Empty groove condition

(b) Design water depth condition
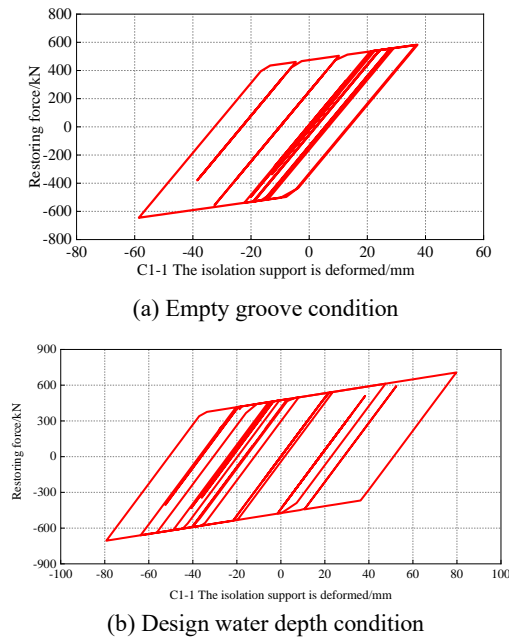
Figure 8. Force-displacement curve of isolation bearing
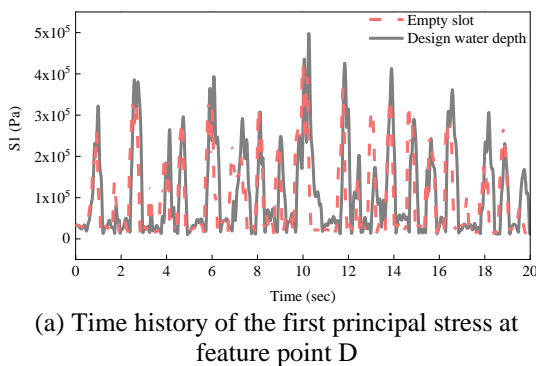
(a) Time history of the first principal stress at feature point D
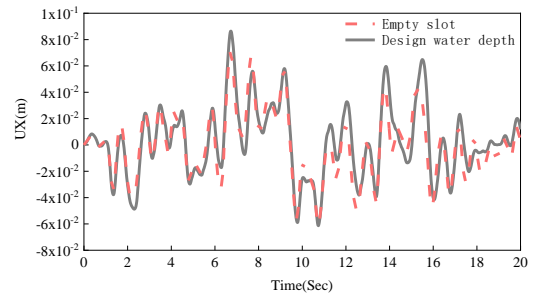
(b) Time history diagram of lateral displacement at feature point D

Figure 9. Time history curve of section feature points

3.5 Response of the upper structure of the tank

In order to explore the performance difference between ordinary support and isolation support, three groups of working conditions are designed according to the actual situation, which are: design water depth - ordinary support, design water depth - isolation support, and empty trough -- isolation support. Three seismic waves are used for dynamic response analysis, respectively. Figure 10 shows the transverse relative displacements between the aqueduct body and support under three different seismic actions. It can be seen from the analysis of Figure 10 that when the isolation bearing is also used, there is little difference between the maximum lateral displacement of the empty trough state and the designed water depth state.
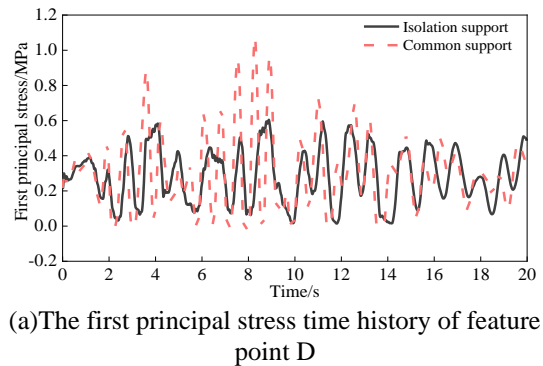
(a)The first principal stress time history of feature point D
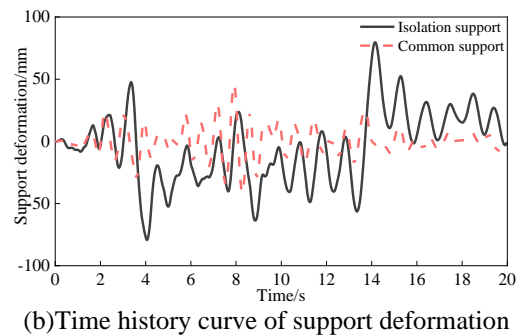
(b)Time history curve of support deformation

Figure 10. Structural response time history curve

Analyzing Figure 10, it can be seen that when the isolation support is also used, there is little difference in the maximum lateral displacement between the empty slot state and the design water depth state; However, when the load is certain and the bearings are different, the maximum lateral displacement of the isolation bearings is about 32mm higher than that of ordinary bearings, while the first principal stress

value of characteristic point D is reduced by about 0.49MPa. Dynamic calculation is carried out with different earthquakes, and the maximum lateral displacement of the bearing under different working conditions is analyzed, as shown in Figure 11.
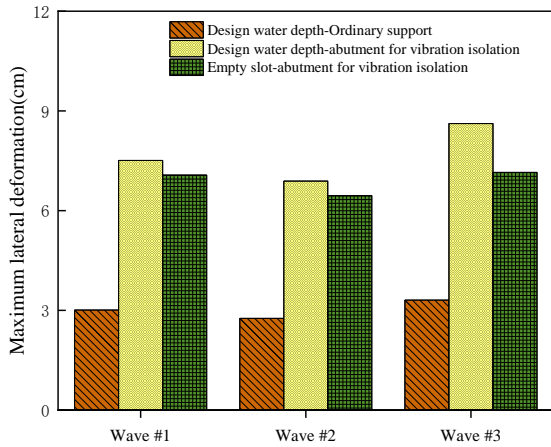
Figure 1. Maximum displacement of different supports

3.6 Internal force situation of slot pier

By integrating the stress of the pier bottom section of the aqueduct, the shear force and bending moment of the pier bottom section are obtained. Select the pier of the third span aqueduct for analysis. Figures 12 (a) and (b) respectively show the shear response at the bottom of the pier and the bending moment response at the bottom of the pier.
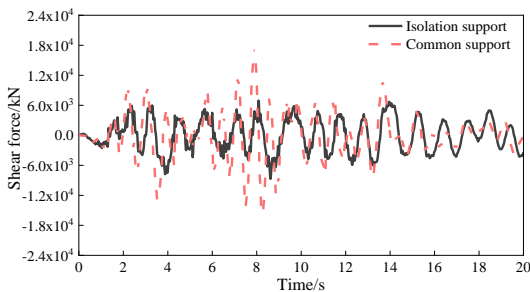
(a) Time history curve of shear force at the bottom of slot pier
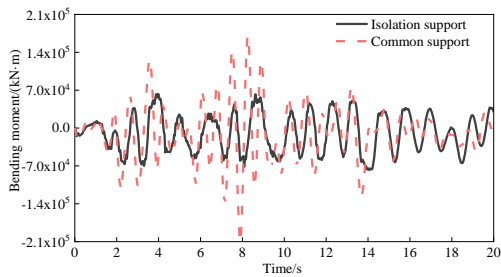
(b) Time history curve of bending moment at the bottom of slot pier

Figure 12. Moment shear time history curve of slot pier

Analyzing Figure 12 (a), it can be seen that in the early stage of seismic excitation, the shear time history curve of the aqueduct using ordinary bearings is significantly higher than

that of the pier using vibration isolation bearings. Compared with ordinary bearings, under the same seismic excitation, isolation bearings significantly reduce the shear force of the pier, with a maximum reduction of 51.1%. At the end of the seismic excitation period, the vibration tends to be gentle, and the displacement amplitude of the support is relatively small. The damping effect of the isolation support is not fully utilized.

Analyzing Figure 12 (b), it can be seen that in the early stage of seismic excitation, the bending moment time history curve of the aqueduct using ordinary bearings is significantly higher than that of the pier using vibration isolation bearings. Compared with ordinary bearings, under the same seismic excitation, the isolation bearing significantly reduces the bending moment of the slot pier, with a maximum reduction of 63.1%. At the end of the seismic excitation period, the vibration tends to be gentle, the displacement amplitude of the support is small, and the damping effect of the isolation support is not fully utilized.

3.7 Water stop deformation condition

Figure 13 shows the variation pattern of relative displacement between adjacent aqueduct sections under empty channel conditions and design water depth conditions. Figure 13 (a) shows the displacement of adjacent aqueduct sections when encountering the first, second, and third waves respectively under empty channel conditions; Figure 13 (b) shows the relative displacement of adjacent aqueduct sections when encountering the first, second, and third waves at the design water depth. From Figure 13 (a), it can be seen that the trends of the three curves under the empty channel condition are basically consistent. During the vibration process, the displacement between the second and third sections of the aqueduct is the largest, reaching a maximum of 0.31mm. From Figure 13 (b), it can be seen that the trends of the three curves are not consistent under the design water depth condition. During the vibration process, the relative displacement between the second and third sections of the aqueduct is the largest, reaching a maximum of 0.41mm.

According to the standard "Polymer Waterproof Materials - Part 2: Waterstops", the elongation at break of rubber waterstops should not be less than 380%. In this study, the water stop width between each slot is 40mm. When the slot is empty, the elongation of the water stop is only 0.823%. When the water depth is designed, the elongation of the water stop is 1.08%, which is far less than the standard requirements, and the water stop will not be damaged.
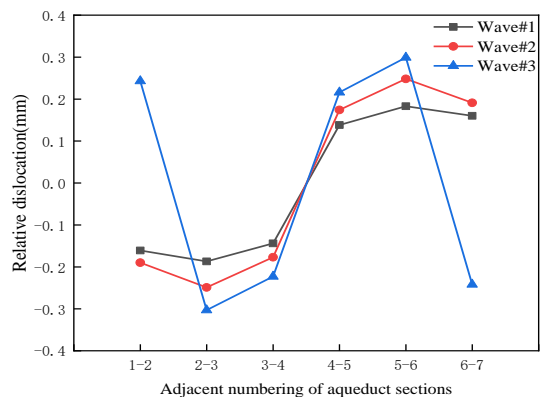
(a) Empty slot
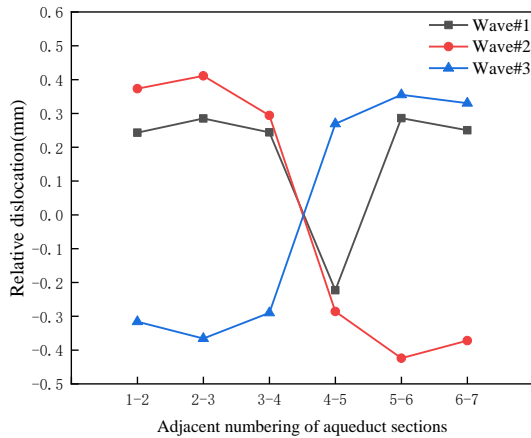
(b) Design water depth

Figure 13. Maximum relative displacement of each adjacent aqueduct segment

4. CONCLUSION

Introducing high damping isolation bearings into the structural system of large aqueducts can effectively reduce the destructive effect of strong earthquakes on large aqueducts. The calculation results of dynamic characteristics indicate that the first step rate of the aqueduct is about 4.323Hz, the first period is about 1.033s, and the acceleration design response spectrum is taken as the maximum value. The dynamic response is too large, which is not conducive to the seismic resistance of the structure. By using damping bearings, the fundamental frequency has been reduced by 82%, increasing the basic period of the aqueduct structure and reducing the response of ground motion to the channel, resulting in a decrease in the response value of the upper structure under earthquake action. By searching for the maximum response value of the entire field of the excitation full time domain aqueduct, the extreme value of the dynamic response of the aqueduct structure can be given. From the analysis results, it can be seen that the stress is generally within the design strength of the concrete, and the water stop deformation also meets the deformation limit specified in the standard. Under the design seismic intensity of the site, the aqueduct structure is relatively safe. The distribution of relative displacement of adjacent aqueduct sections has a certain regularity along the longitudinal direction. The overall vibration distribution is "strong -weak -strong", and due to the severe dislocation of

adjacent groove sections on both sides, increasing the water stop can strengthen the performance of weak parts. Due to the limitations of using numerical simulation methods to simulate the application of isolation bearings on aqueducts, the accuracy of the results will be verified through experiments in the future.

REFERENCES

[1] Fan, L., Wang, Z. (2001). Design of bridge seismic reduction and isolation. China Communications Press, pp. 20-30.

[2] Xu, J., Chen, H. (2008), Wang Bo Research on Nonlinear Isolation of Aqueduct Structures. Journal of Yangtze River Scientific Research Institute, (4): 61-64.

[3] Hengshui Fengze Engineering Rubber Technology Development Co. (2006). Bridge engineering fittings.

[4] Zhou, H., Ma, J., Ma, J. (2007). The development of domestic and foreign ferries and the South-to-North Water Diversion Central Line Caohe River Ferry. South-to-North Water Transfers and Water Science and Technology, (03): 14-17, 20. https://doi.org/10.13476/j.cnki.nsbdqk.2007.03.006

[5] Wang, H., Lu, X., Yuan, S. (2014). Numerical simulation of lead rubber bearing effect on aqueduct isolation based on ADINA. Journal of East China Jiaotong University, (01): 114-118. https://doi.org/10.16749/j.cnki.jecjtu.2014.01.017

[6] Ding, X., Peng, J., Yin, K.(2016). Design and isolation performance of aqueduct with double spherical seismic isolation bearing. Water Resources and Power, (07): 80-83.

[7] He, J., You, L., Li, S.(2019). Study on seismic isolation design of beam aqueduct in high intensity area. Water Resources Planning and Design, (09): 140-146.

[8] Zhang, D., Li, J., Wang, Q.(2021). Dynamic calculation and seismic isolation research of large-scale aqueducts based on "design standards". Journal of Hydraulic Engineering, (07): 873-883. https://doi.org/10.13243/j.cnki.slxb.20200851

[9] Han, Z., Ao, X., Pan, P.(2023). Seismic and isolation analysis of a large span elevated beam aqueduct. Journal of Yangtze River Scientific Research Institute, pp. 1-10.

[10] Ministry of Housing and Urban-Rural Construction of the People's Republic of China. (2018). GB51247-201, Standard for seismic design of hydraulic structures. Beijing: China Planning Press.